


Ultrahigh Quality Factor Photonic Nanojets Generated by Truncated Microtoroid Structures

Yajie Chen, Ying Wang, Xintao Zeng, Shifa Pan, Musheng Chen, Yongxi Zeng, Baoyu Fu, Pinghui Wu , and Miao Pan

Abstract—A photonic nanojet (PNJ) is a highly confined light beam that focuses from the shadow side of microparticles. In 46.47 λ this work, we propose a PNJ with ultrahigh quality factor formed by dielectric truncated microtoroid. The key properties of PNJ, such as the maximum intensity, the length of PNJ, the full-width at half maximum (FWHM), are studied in detail using finite-difference time-domain (FDTD) analysis. The results show that a PNJ with an enhanced intensity of 55.21 times to the incident light, superlong length of 46.47 λ and subwavelength FWHM of 0.77 λ is formed by semi-microtoroid, thus, an ultrahigh quality factor of 3308.68 is achieved. More importantly, the properties of the PNJ are tunable by changing the truncated proportions of the microtoroid. The structure we proposed has the advantages of compact structure and simple experimental operation, which is expected to apply in many research fields, including optical detection, optical data storage, super-resolution image, nanopattern, nanolithography, and so on.

Index Terms—Photonic nanojet, truncated microtoroid, quality factor, FDTD.

I. INTRODUCTION

A PHOTONIC nanojet (PNJ) is a tightly focused light beam with a high-intensity peak, long length and subwavelength waist that emerges from the shadow surface of a transparent microparticle. The first report of this phenomenon is Benincasa et al. in 1987 [1]. The conception of PNJ is proposed by Chen et al. in 2004 [2]. Since then, the PNJs have attracted much attentions of researchers for its potential applications, including nanoparticles sensing [3]–[5], all optical switch [6], optical subwavelength detection [7]–[9], optical data storage [10], super-resolution image [11]–[14], and orbital angle momentum [15].

Manuscript received May 31, 2021; revised July 10, 2021; accepted July 21, 2021. Date of publication July 27, 2021; date of current version August 10, 2021. This work was supported in part by the National Natural Science Foundation of China under Grant 11704223, in part by the Natural Science Foundation of Fujian Province under Grants 2018J05008, 2019J01736, and 2020J01777, and in part by the Distinguished Young Scholars Program of Fujian Province under Grant C18032. (Corresponding author: Pinghui Wu and Miao Pan.)

The authors are with the Research Center for Photonic Technology, Fujian Provincial Key Laboratory for Advanced Micro-nano Photonics Technology and Devices & Key Laboratory of Information Functional Material for Fujian Higher Education, Quanzhou Normal University, Quanzhou 362000, China (e-mail: cheney_jie@outlook.com; ailsa_ying0316@outlook.com; zeng_xintao@163.com; panshifa@qztc.edu.cn; mushengchen@163.com; clmzyx@163.com; fubaoyu@qztc.edu.cn; phwu@zju.edu.cn; miao_pan@qztc.edu.cn).

Digital Object Identifier 10.1109/JPHOT.2021.3100136

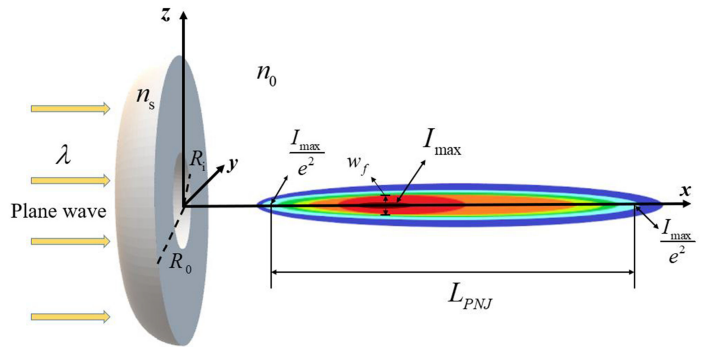


Fig. 1. Schematic diagram of truncated microtoroid structure to generate PNJ.

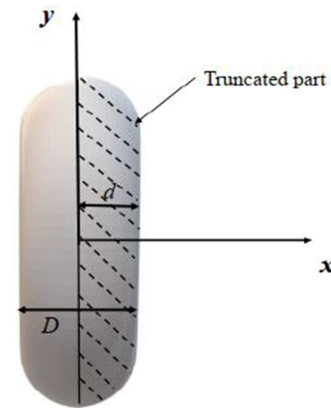


Fig. 2. The xoy plane view of the truncated microtoroid structure.

Many demonstrations show that the key properties of the PNJ, including maximum intensity, the length of PNJ, and FWHM, depend on the geometric parameters (size, shape, etc.), refractive indices of the micro-particles and output wavelength of the incident light [16]–[20]. For these applications, the enhanced electric field intensity, the ultralong length of PNJ and narrow beam waist of PNJs are especially expected by researchers. Traditionally, the microsphere or microcylinder is employed to form PNJ [21]–[24]. However, the generate point, which means the position where PNJ firstly formed, is very close to the shadow surface of the microstructure in these cases, which constrict the applications where need long working distance. In order to improve the quality of PNJ, other geometric structure, such as microcuboid [25], [26], microfiber [27], [28], microtoroid [29] and microaxicon [30], are proposed for generating of PNJs.

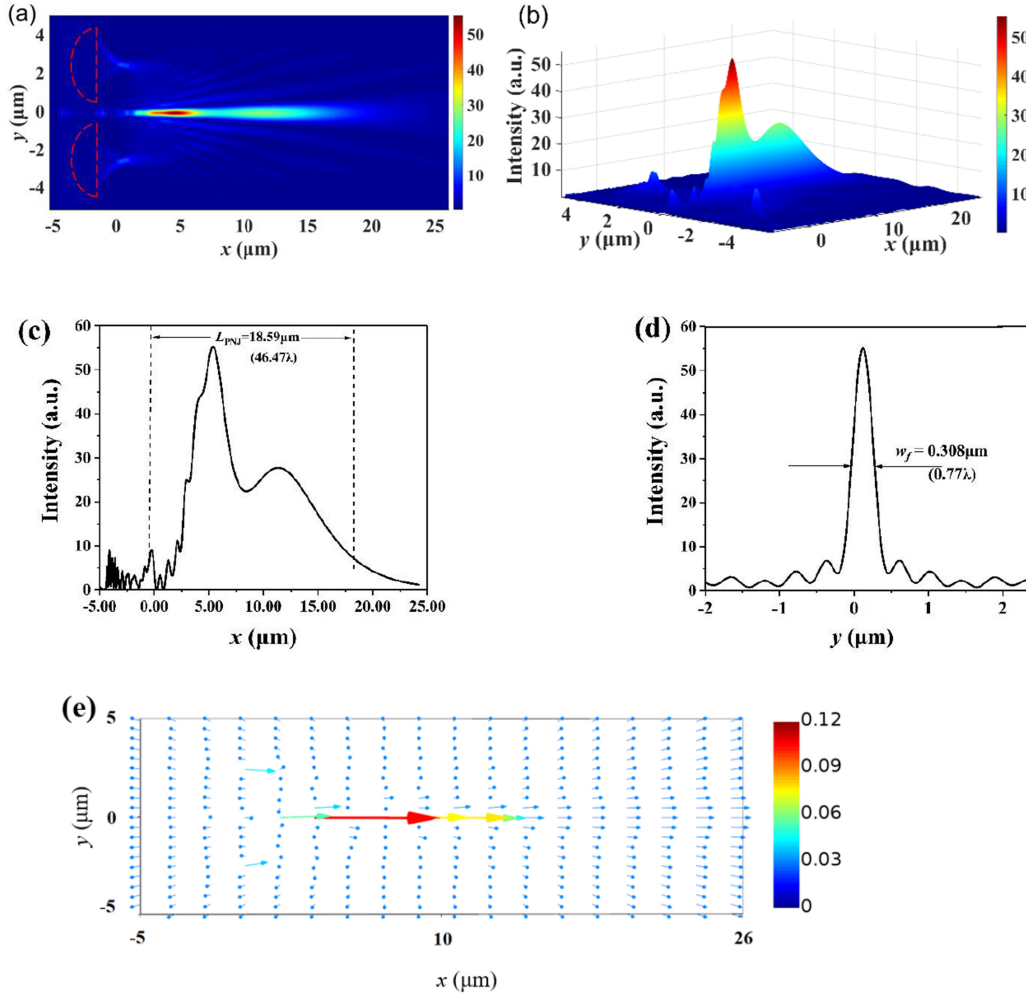


Fig. 3. The PNJ generated by semi-microtoroid: (a) electric field intensity distribution, (b) 3D electric field intensity distribution, (c) the length of PNJ, (d) the FWHM of PNJ, (e) power flow of the PNJ.

In this paper, we design truncated- microtoroids with different truncated proportions to generate PNJs using finite-difference time-domain (FDTD) simulations. The dielectric microtoroid can be fabricated by the technique of short-pulse CO_2 -laser reflow treatment, which is studied in the researches of microtoroid and micro-resonators [29], [31]. The XeF_2 dry etching and the CO_2 laser exposure also can fabricate such a microtoroid [32]. And then, the focused ion beam (FIB) method [33], [34] is applied to the microtoroid structure to fabricate truncated microtoroid with different height. A PNJ with an enhanced intensity of 55.21 times to the incident light, ultralong length up to 46.47λ , narrow FWHM of 0.77λ and high quality factor of 3308.68 generated by the semi-microtoroid. Moreover, the key properties of PNJs are tunable by changing the different truncated proportions, which means the proposed structure can adapt to different application fields, including optical detection, optical data storage, super-resolution image, nanopattern, nanolithography and biomedical imaging. Compare with the traditional microsphere and microcylinder structures, the PNJ generated from truncated microtoroid structure has long working distance and higher maximum intensity. What is also worth mention that the truncated microtoroid is height-tunable compare with traditional microtoroid or microaxicon.

II. STRUCTURE AND METHOD

The properties of PNJ, including maximum intensity, PNJ length and FWHM, depend significantly on the dimension and material of the microparticle. Fig. 1 shows the schematic of photonic nanojet generated by the proposed truncated microtoroid structure. The plane wave with a wavelength $\lambda = 400$ nm is injected to the surface of the truncated microtoroid along x axis forward direction. R_o and R_i are the outer and inner radius of the truncated microtoroids, which is set as 4λ and λ respectively. n_o is the refractive index of background medium, in this case we assume it as air, that is, $n_o = 1$. Here, n_s , the refractive index of the truncated microtoroid, is set as 1.47, which encounter the refractive index of silica in 400 nm. As for the properties of PNJ, I_{\max} is maximum intensity, which means the enhancement compare with the incident light. L_{PNJ} is the length from the point of $1/e^2$ value of I_{\max} in the formed side to the point of the $1/e^2$ value of I_{\max} in the decay side. w_f stands for full width at half maximum (FWHM), means the waist diameter of the PNJ.

To better understand of the truncated proportion, the xoy view of the proposed structure is shown in Fig. 2. The length of whole microtoroid is set as $D = 10\lambda$, and the microtoroid is truncated by different proportions d (5λ in Fig. 2) in order to generating

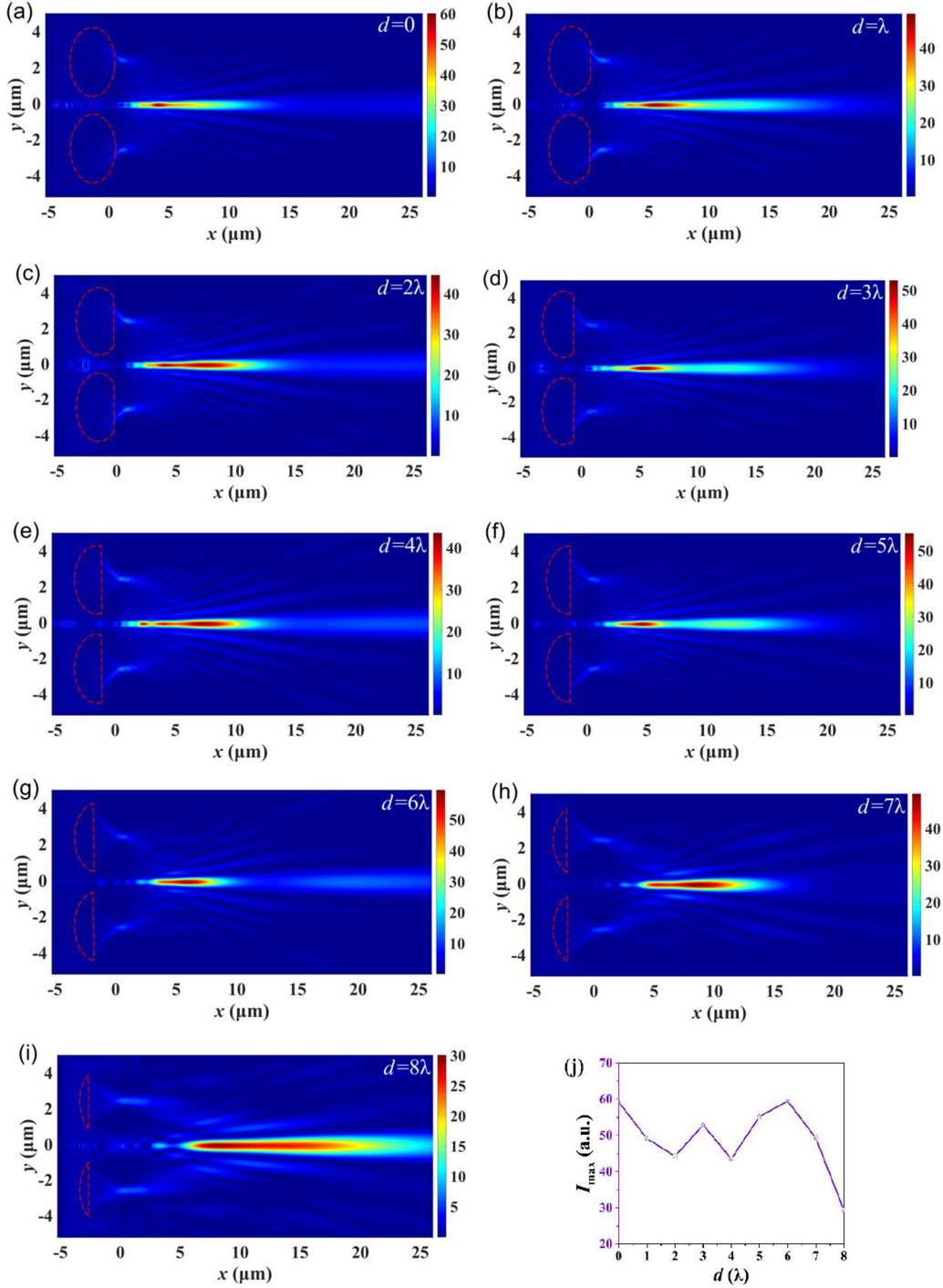


Fig. 4. Electric field intensity distribution of the PNJs formed by truncated microtoroid structure with different truncated proportions: (a) $d = 0$, (b) $d = \lambda$, (c) $d = 2\lambda$, (d) $d = 3\lambda$, (e) $d = 4\lambda$, (f) $d = 5\lambda$, (g) $d = 6\lambda$, (h) $d = 7\lambda$, and (i) $d = 8\lambda$. (j) maximum intensity differences of the PNJ formed by truncated microtoroid structure with different truncated proportions.

PNJ with different properties, which is discussed in detail in next part.

III. RESULTS AND DISCUSSIONS

The simulations of photonic nanojets generated by truncated microtoroid are employed by using the finite-difference time-domain (FDTD) method. In order to ensure the accuracy of the calculation, the simulation region is set up to be

$31 \mu\text{m} \times 10 \mu\text{m} \times 10 \mu\text{m}$ and non-uniform mesh with minimum mesh step of 0.25 nm is applied. Perfectly matched layers (PML) are arranged around the boundaries.

To begin with, we investigate a case of semi-microtoroid, that is, $d = D/2$. Fig. 3(a) shows the electric field intensity distribution of PNJ generated by the semi-microtoroid and Fig. 3(b) show a three-dimension (3D) of the electric field intensity distribution. From figs 3(a) and 3(b), we can roughly recognize that the maximum intensity of the PNJ generated

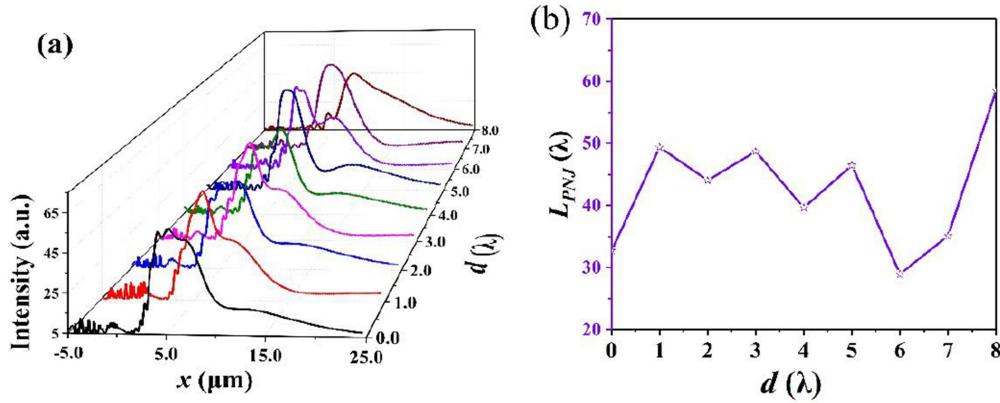


Fig. 5. (a) The length of PNJs along x axis formed by truncated microtoroid structure with different truncated proportions; (b) the length differences of PNJs formed by truncated microtoroid structure with different truncated proportions.

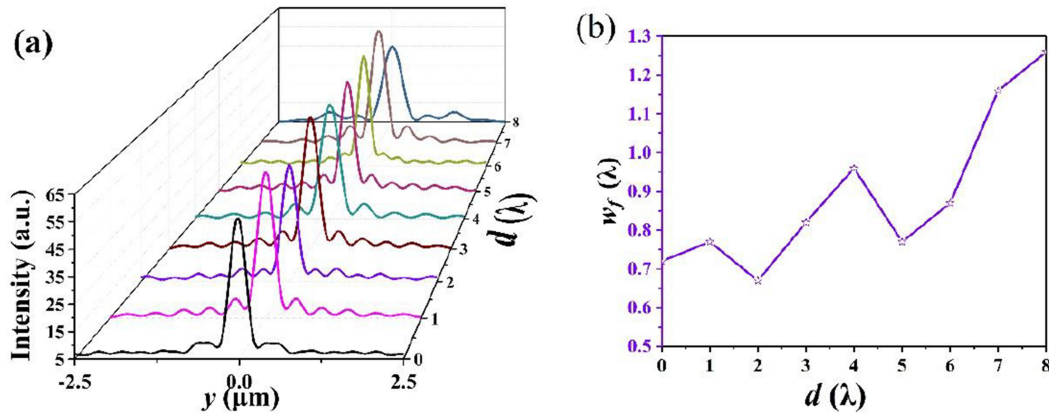


Fig. 6. (a) The FWHM of PNJs along y axis formed by truncated microtoroid structure with different truncated proportion; (b) the FWHM differences of PNJs formed by truncated microtoroid structure with different truncated proportion.

from the semi-microtoroid is ~ 50 times of incident light, which is a large enhancement. It is also worth mentioning that the PNJ generated far away from the shadow surface of the semi-microtoroid. Fig. 3(c) gives the axial electric field intensity, the length of PNJ formed by the semi-microtoroid is $18.59 \mu\text{m}$ ($\sim 46.47\lambda$). The distribution of the PNJ along y axis is depicted in Fig. 3(c), which gives the subwavelength FWHM of the PNJ formed by the semi-microtoroid of $0.308 \mu\text{m}$ (0.77λ). To better understand the mechanism of the PNJ formed by the proposed truncated microtoroid structure, we investigate the power flow of semi-microtoroid in Fig. 3(e). The energy flow of the incident light is deflected by the truncated microtoroid and then converges. A collimation of the incident field by the microtoroid, and interferences between the field scattered by the dielectric microtoroid and the incident field can form the focused beam with small diffraction.

For general research, the PNJs generated by the microtoroids truncated in different proportions are investigated. Here, D is supposed as 10λ , the d varies from 0 to 8λ in an interval of λ . Fig. 4(a)-(i) give the electric field intensity distribution results of PNJs generated by truncated microtoroids with different truncated proportions d . We can find out that the PNJs generated by all cases have a large intensity enhancement to the

incident light, and the lengths of PNJs are large than $5 \mu\text{m}$ (10λ). The maximum intensity of PNJ variance caused by different truncated proportions is shown in Fig. 4(j). We can see from Fig. 4(j) that the microtoroids with truncated proportions $d = 0$ and 6λ get the maximum of ~ 59 times enhancement to the incident light. However, when the truncated proportion $d = 8\lambda$, the maximum intensity of PNJ shrinks to 29.3 times of incident light.

As for the research on the length and FWHM of PNJs generated from different proportions, the results are shown in Fig. 5 and Fig. 6. All the results are normalized to λ . As shown in Fig. 5(a), it can be seen clearly the length of PNJs changes due to the different truncated proportions. For quantitative analysis, the length of PNJs is summarized in Fig. 5(b). It is shown that the length of PNJ varies from 25λ to 60λ . When the truncated proportion $d = 8\lambda$, the length of PNJ reaches its maximum of 58.57λ . The PNJs generated by truncated microtoroid with $d = \lambda$, $d = 3\lambda$ and $d = 5\lambda$ also have long PNJ length of $\sim 50\lambda$. Fig. 6 shows the FWHM with different truncated proportions. As depicted in Fig. 6(b), the FWHM of PNJs fluctuate from 0.6λ to 1.3λ and get its minimum of 0.67λ with $d = 2\lambda$. What is also worth mention that the FWHMs get large than λ when the truncated proportions $d = 7\lambda$ and 8λ .

TABLE 1
THE PROPERTIES OF PNJS WITH DIFFERENT TRUNCATED PROPORTIONS

d (λ)	I_{\max} (a. u.)	L_{PNJ} (λ)	w_f (λ)	Q
0	59.26	32.70	0.72	2665.68
1	49.18	49.40	0.77	3132.80
2	44.28	44.05	0.67	2874.77
3	52.90	48.72	0.82	3128.09
4	43.51	39.65	0.96	1779.44
5	55.21	46.47	0.77	3308.68
6	59.51	28.95	0.87	1974.57
7	49.32	35.12	1.16	1488.92
8	29.30	58.57	1.26	1361.44

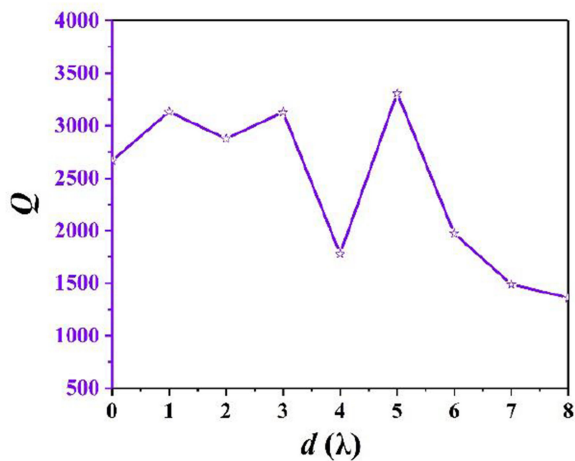


Fig. 7. The quality factor differences of PNJs formed by truncated microtoroid structure with different truncated proportions.

In order to evaluate the property of PNJ generated by the proposed structure more comprehensively, the quality factor Q of PNJ is defined as [35]

$$Q = \frac{I_{\max} \cdot L_{\text{PNJ}}}{w_f} \quad (1)$$

where the I_{\max} , L_{PNJ} , and w_f are defined as the maximum intensity, the length of PNJ, and the FWHM, respectively. Fig. 7 gives the quality factor Q differences of PNJs with different truncated proportions d . When $d = 4, 7, 8\lambda$, the Q shrink to less than 2000. We can find that Q reaches its maximum of 3308.68 when $d = 5\lambda$, which means the PNJ has a great quality with semi-microtoroid structure. To our best knowledge, this is the highest quality factor PNJ produced from a microparticle that has been reported until now.

To summarize, Table 1 shows the properties of PNJs with different d . Three key properties of PNJ, I_{\max} , L_{PNJ} , w_f , are listed in this table. With these three parameters changes, the Q varies from 1361.44 with $d = 8\lambda$ to 3308.68 with $d = 5\lambda$.

Obviously, the parameters of PNJ can be modified flexibly by changing the truncated area for more practical applications.

IV. CONCLUSION

In this paper, we designed a truncated microtoroid to generate PNJs using finite-difference time-domain (FDTD) simulations. Three key parameters of PNJ, maximum intensity, FWHM, and the length of PNJ, is studied in detail. A PNJ with a magnified electric field intensity of 55.21 times to the incident light, ultralong length of 46.47λ and subwavelength FWHM of 0.77λ is formed by semi-microtoroid. Moreover, the truncated proportion is adjusted to generate PNJ with different properties. Finally, the quality factor quality factor is defined to judge the quality of the PNJs and we concluded that the semi-microtoroid generated PNJ has the best quality among this study. To our best knowledge, this is the highest quality factor among the published researches. The properties of PNJ can be modified flexibly by changing the truncated proportions for more practical applications, including nanopatterning, optical sensing, micro-manipulations, and so on.

REFERENCES

- [1] R. K. Chang, D. S. Benincasa, P. W. Barber, J. Z. Zhang, and W. F. Hsieh, "Spatial distribution of the internal and near-field intensities of large cylindrical and spherical scatterers," *Appl. Opt.*, vol. 26, pp. 1348–1356, 1987.
- [2] C. Zhigang, T. Allen, and B. Vadim, "Photonic nanojet enhancement of backscattering of light by nanoparticles: A potential novel visible-light ultramicroscopy technique," *Opt. Exp.*, vol. 12, no. 7, pp. 1214–1220, 2004.
- [3] G. Gu, J. Song, C. Ming, P. Xiao, H. Liang, and J. Qu, "Single nanoparticle detection using a photonic nanojet," *Nanoscale*, vol. 10, no. 29, pp. 14182–14189, 2018.
- [4] C. M. Ruiz and J. J. Simpson, "Detection of embedded ultra-subwavelength-thin dielectric features using elongated photonic nanojets," *Opt. Exp.*, vol. 18, pp. 16805–16812, 2012.
- [5] S. C. Kong, A. Taflove, and V. Backman, "Quasi one-dimensional light beam generated by a graded-index microsphere: Errata," *Opt. Exp.*, vol. 18, pp. 3973–3979, 2010.
- [6] B. Born, J. Krupa, S. Geoffroy-Gagnon, and J. F. Holzman, "Integration of photonic nanojets and semiconductor nanoparticles for enhanced all-optical switching," *Nature Commun.*, vol. 6, pp. 8097–8104, 2015.

- [7] H. Yang, M. Cornaglia, and M. Gijs, "Photonic nanojet array for fast detection of single nanoparticles in a flow," *Nano Lett.*, vol. 15, pp. 1730–1743, 2015.
- [8] S. Yang, A. Taflove, and V. Backman, "Experimental confirmation at visible light wavelengths of the backscattering enhancement phenomenon of the photonic nanojet," *Opt. Exp.*, vol. 19, pp. 7084–7093, 2011.
- [9] Y. Li, H. Xin, X. Liu, Y. Zhang, H. Lei, and B. Li, "Trapping and detection of nanoparticles and cells using a parallel photonic nanojet array," *ACS Nano*, pp. 5800–5808, 2016.
- [10] S. C. Kong, S. Alan, T. Allen, and B. Vadim, "Photonic nanojet-enabled optical data storage," *Opt. Exp.*, vol. 16, no. 18, pp. 13713–13719, 2008.
- [11] L. Chen, Z. Yan, M. Wu, and M. Hong, "Remote-mode microsphere nanoimaging: New boundaries for optical microscopes," *Opto-Electron. Adv.*, vol. 1, pp. 17000101–17000107, 2018.
- [12] C. Y. Liu and K. L. Hsiao, "Direct imaging of optimal photonic nanojets from core-shell microcylinders," *Opt. Lett.*, vol. 40, no. 22, pp. 5303–5306, 2015.
- [13] Y. L. Ju *et al.*, "Near-field focusing and magnification through self-assembled nanoscale spherical lenses," *Nature*, vol. 460, no. 7254, pp. 498–501.
- [14] G. Huszka, Y. Hui, and M. Gijs, "Microsphere-based super-resolution scanning optical microscope," *Opt. Exp.*, vol. 25, pp. 15079–15092, 2017.
- [15] Y. Zhou, H. Gao, J. Teng, X. Luo, and M. Hong, "Orbital angular momentum generation via a spiral phase microsphere," *Opt. Lett.*, vol. 43, pp. 34–37, 2018.
- [16] Y. Yang, V. A. Zenin, and S. I. Bozhevolnyi, "Anapole-assisted strong field enhancement in individual all-dielectric nanostructures," *ACS Photon.*, vol. 5, pp. 1960–1966, 2018.
- [17] Z. Zhen, Y. Huang, Y. Feng, Y. Shen, and Z. Li, "An ultranarrow photonic nanojet formed by an engineered two-layer microcylinder of high refractive-index materials," *Opt. Exp.*, vol. 27, pp. 9178–9185, 2019.
- [18] C.-Y. Liu and C.-J. Chen, "Characterization of photonic nanojets in dielectric microdisks," *Physica E: Low-dimensional Syst. Nanostructures*, vol. 73, pp. 226–234, 2015.
- [19] Y. E. Geints, A. A. Zemlyanov, and E. K. Panina, "Controlling the parameters of photon nanojets of composite microspheres," *Opt. Spectrosc.*, vol. 109, pp. 590–595, 2010.
- [20] Y. Yang, V. A. Zenin, and S. I. Bozhevolnyi, "Anapole-assisted strong field enhancement in individual all-dielectric nanostructures," *ACS Photon.*, vol. 5, pp. 1960–1966, 2018.
- [21] Y. Shen, L. V. Wang, and J. T. Shen, "Ultralong photonic nanojet formed by a two-layer dielectric microsphere," *Opt. Lett.*, vol. 39, pp. 4120–4123, 2014.
- [22] J. Yang, P. Twardowski, P. Gérard, D. Yi, and S. Lecler, "Ultra-narrow photonic nanojets through a glass cuboid embedded in a dielectric cylinder," *Opt. Exp.*, vol. 26, pp. 3723–3731, 2018.
- [23] S. Zhou and T. Zhou, "An ultra-narrow photonic nanojet generated from a high refractive-index micro-flat-ended cylinder," *Appl. Phys. Exp.*, vol. 13, pp. 042010–042020, 2020.
- [24] P. Wu, L. Jia, K. Wei, and W. Yue, "Tunable and ultra-elongated photonic nanojet generated by a liquid-immersed core-shell dielectric microsphere," *Appl. Phys. Exp.*, vol. 8, no. 11, pp. 112001–03, 2015.
- [25] C. Nayak and A. Saha, "Effect of the matrix dimension on the performance of photonic nanojets produce from an array of cuboid profile microsteps," *Optik*, vol. 127, pp. 10766–10771, 2016.
- [26] L. Cheng-Yang, Y. Tzu-Ping, V. Oleg, I. Minin, and M. V., "Engineering photonic nanojet by a graded-index micro-cuboid," *Physica, E: Low-Dimensional Syst. & Nanostructures*, vol. 98, pp. 105–110, 2018.
- [27] R. Pierron, J. Zelgowski, P. Pfeiffer, J. Fontaine, and S. Lecler, "Photonic jet: Key role of injection for etchings with a shaped optical fiber tip," *Opt. Lett.*, vol. 42, pp. 2707–2712, 2017.
- [28] J. Dise and A. Darafsheh, "Characterization of photonic nanojets formed by dielectric microfibers," in *Proc. Integr. Opt.: Devices, Materials, and Technologies XXIII*, US, 2019, pp. 71.
- [29] B. Zhang, J. Hao, S. Zhe, H. Wu, and J. Ding, "Ultralong photonic nanojet formed by dielectric microtoroid structure," *Appl. Opt.*, vol. 57, pp. 8331, 2018.
- [30] H. He, S. Chen, H. Zou, Q. Li, and X. Wu, "Fabrication of micro-axicons using direct-laser writing," *Opt. Exp.*, vol. 22, no. 9, pp. 11035–11042, 2014.
- [31] K. A. Knapper, K. D. Heylman, E. H. Horak, and R. H. Goldsmith, "Chip-scale fabrication of high-Q all-glass toroidal micro resonators for single-particle label-free imaging," *Advance Mater.*, vol. 28, pp. 2945–2950, 2016.
- [32] M. Hossein-Zadeh, and K. J. Vahala, "Free ultra-high-Q microtoroid: A tool for designing photonic devices," *Opt. Exp.*, vol. 15, no. 1, pp. 166–175, 2007.
- [33] S. Zhang, D. Wu, and L. Zhou, "Characterization of controlled release microspheres using FIB-SEM and image-based release prediction," *AAPS Pharm Sci Tech*, vol. 21, no. 5, 2020.
- [34] B. Li, X. Tang, H. Xie, and Z. Xin, "Focused ion beam (FIB) nanomachining and FIB moire technique for strain analysis in MEMS/NEMS structures and devices," in *Proc. IEEE 16th Int. Conf. Micro Electro Mech. Syst.*, 2003.
- [35] C. Y. Liu, T. P. Yen, O. V. Minin, and I. V. Minin, "Engineering photonic nanojet by a graded-index micro-cuboid," *Physica E*, vol. 98, pp. 105–110, 2018.